Modeling Ash Fall and Debris Flow Hazards of Mt Erebus, Antarctica

A GIS Approach

Cameron Asher

February/March 2014

Mt Erebus is a volcano in the Ross Sea that has been active since its first sighting in 1841 by Captain James Clark Ross. It consistently maintains an eruption plume and convecting lava lake of phonolitic composition, and regularly erupts as minor strombolian events. Prior to observations of Erebus beginning, major eruption events have occurred, with 2 plinian eruptions depositing ash up to 200km from the vent, and >43 eruptions depositing ash at least 7-12km from source. Using this information, three volcanic eruptions are modelled to predict ash fall using various wind speeds, and assuming an eruption plume of 7000m, and an erupted mass of $1x10^{10}$kg. It is observed that debris flows will most likely follow glacier paths as these already follow the lowest topographical route, while the eruption modelled with have little impact on Scott Base or McMurdo Station, unless optimal wind conditions occur.

Contents

Tables

Introduction

This study aims to investigate some of the volcanic hazards that may be experienced at Mt Erebus in the future. The study has two principal investigation paths:

- Model ash fall based on parameters from eruptions similar to the possible eruptions from Mt Erebus.
- Model potential debris flow[1] paths in relation to ash fall volume, under the premise that a catchment with a greater volume of erupted material has a greater remobilization potential.

While there has been a limited amount of historic volcanic activity that has affected anywhere other than the main crater of Mt Erebus, geologic evidence shows that large eruption events have occurred in the past, and may happen again in the future. By developing these models we can plan and act to prevent negative impact to human activities, infrastructure, and life.

Geological Setting

Mt Erebus, and Ross Island, are part of the McMurdo Volcanic Group (from Harrington (1958) which includes all Cenozoic volcanic rocks within the Ross Sea and Ross Ice Shelf (collectively known as the Ross Embayment) and sits along the flanks of the Western Antarctic rift system. Kyle & Cole (1974) subdivided the MVG into four provinces: Hallet, Melbourne, Erebus, and the now excluded Balleny. This division was based on spatial distribution and tectonic setting. Relative to the other provinces, extensive research has focuses on the Erebus Volcanic Province (EVP) making it the best known province in the MVG (LeMasurier & Thomson, 1990).

The MVG is stratigraphically important as it is the first terrestrial record of the Transantarctic Mountains since the Jurrasic aged Ferrar Supergroup. The oldest dated extrusive in the MVG is a lava from Sheridan Bluff (19.8Ma) while the oldest dated intrusive is an alkaline intrusive in the Melbourne Volcanic Province (25Ma; Kyle, 1990).

Kyle (1990) categorised the volcanics of the MVG into three major volcanic forms (which apply roughly to almost all volcanic provinces worldwide):

1. **Basaltic Shield Volcanoes**, over 3000m high
2. **Stratovolcanoes**, dominantly trachytic or phonolitic in compostion
3. **Scoria cones** and **lava flows**, small, isolated, and dominantly basaltic. These often occur as late-stage, parasitic cones on shield and stratovolcanoes.

Kyle also noted that basaltic volcanoes may coalesce along fractures to form linear, elongate features, such as Hut Point Peninsula on Ross Island and the Adare Peninsula, while Kyle & Cole (1974) noted a radial symmetry around volcanic centres (eg. Mt Erebus and Mt Discovery), which may suggest crustal doming from the inferred hotspot responsible for volcanism in the southern Ross Sea.

[1] Debris flow here refers mainly to lahars and hyperconcentrated flows directly related to volcanic activity, although to avoid confusion with multiple descriptive terminologies and classification schemes, the term debris flow is used throughout this study.

Mt Erebus is the southernmost active volcano on earth, the most active volcano in Antarctica, and one of two active volcanoes of the McMurdo Volcanic Group, the other being Mt Melbourne in Victoria Land which has weak geothermal activity (Giggenbach, Kyle, & Lyon, 1973; LeMasurier & Thomson, 1990). Mt Erebus sits at the southern end of the Terror Rift (Figure 1), while Mt Melbourne sits at the northern end (Kyle, 1990).

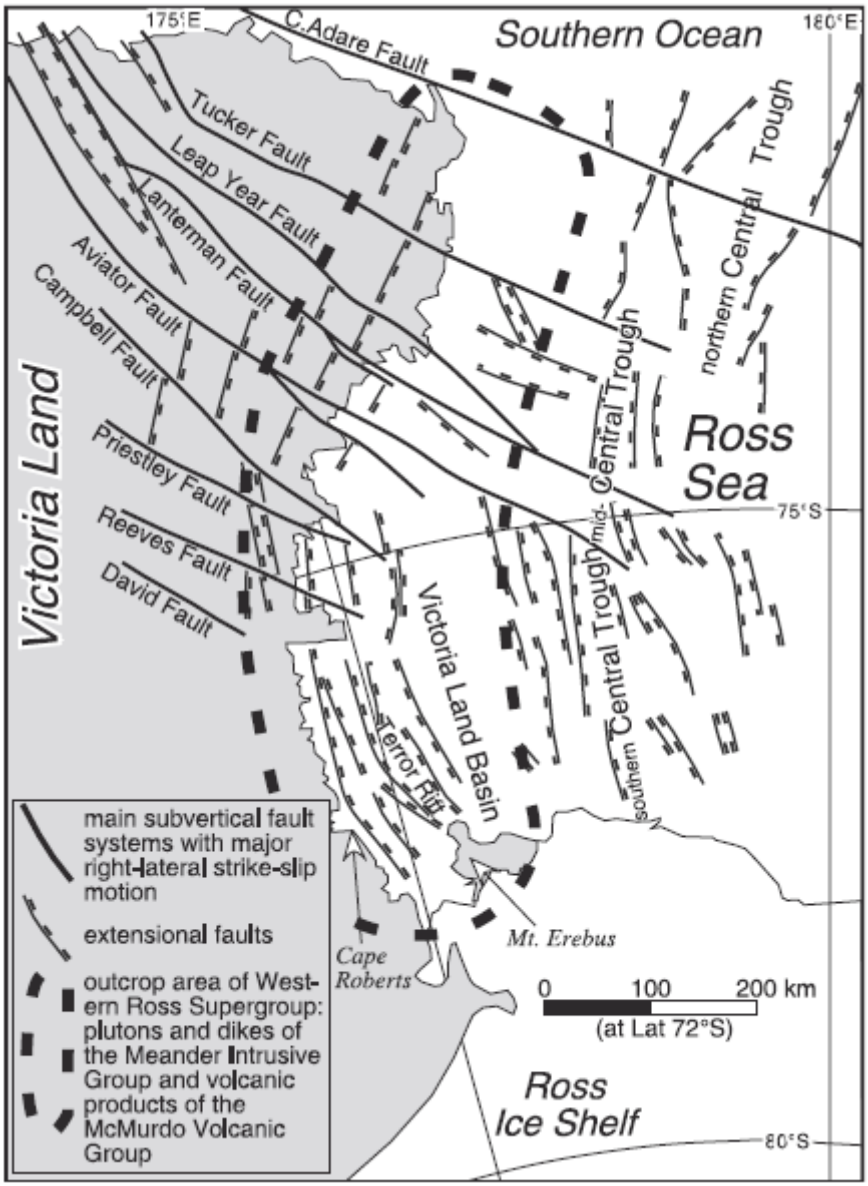

Figure 1. Structural- tectonic map for the Ross Sea area. From Rocchi et al. (2002) and references therein. Ross Island and Mt Erebus is centre bottom.

Volcanic History

Mt Erebus is a stratovolcano reaching an elevation of 3794 m, flanked by the two volcanoes: Mt Bird (1800m, 4000 – 3000 ka, extinct), and Mt Terror (3230m, 1800 -~800 ka, dormant), along with a range of smaller cones and eruptive centres. Surrounding the summit there is an area interpreted as at least one caldera, possibly two, approximately 4km across (figure 2). This has been filled with lavas and pyroclastic deposits of ages ranging between 17±8 to 1±5 ka. Pre-caldera lavas have been dated in two age ranges, 95±9 to 76±4 ka and 27±3 to 21±4ka, putting the age of the 'young' caldera

collapse at between 25 and 11 ka, while the 'old' caldera event may have occurred between 80 and 24 ka (Harpel, Kyle, Esser, McIntosh, & Caldwell, 2004). A geochemical difference is seen between post and pre caldera lavas, with the more recent lavas are of phonolite composition, while pre-caldera lavas range from phonolite to tephriphonolite (Kyle, Moore, & Thirlwirl, 1992).

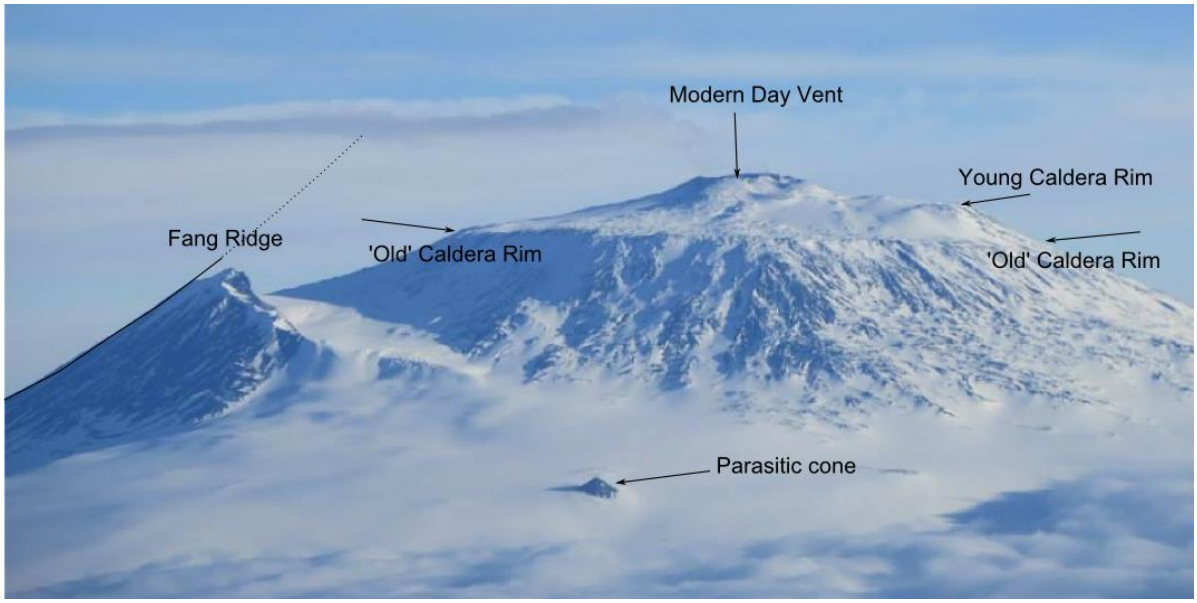

Figure 2.Aerial view of the summit of Erebus, taken from the west looking east. The 'old' caldera rim is easily identifiable, although the 'young' caldera is a bit more difficult to distinguish. The steep back of Fang Ridge can be followed up to estimate the location for the summit of Proto-Erebus. Photo Credit: Beth Vanderhaven.

A prominent ridge to the north of the summit, known as Fang Ridge (Figure 2), is likely the rim of a Proto-Erebus eruption centre and has been dated at between 718±66 to 1070±180 ka (Esser, Kyle, & McIntosh, 2004). Current activity at Erebus consists of a convecting lake of anorthoclase-phonolite lava, the only of its kind on earth, located in a pit crater of the summit crater.

Geological analysis of the volcanic history of Mt Erebus is challenging for a number of reasons:

- Field expeditions are only possible during the austral summer season,
- The environment is very inhospitable and remote, with summer ambient air temperatures averaging ≈ -15˚C and as low as -30˚C during summer (MEVO, 2014),
- Field expeditions are expensive and require great justification to receive funding,
- Much of the volcano is covered in ice and snow, obscuring outcrops (Esser et al., 2004),
- Glaciers, while acting as good preservers for ash fall events, also move and distort the tephra layers, limiting the potential for isopach recreation (Harpel, Kyle, & Dunbar, 2008)
- Lava flows are petrographically indistinguishable with limited geochemical variation (Harpel et al., 2004)
- Tephra layers are prone to sub-aerial erosion from the frequent high velocity winds.

Due to these factors, geological mapping of Mt Erebus is more limited than volcanoes on other continents.

Erebus Building Phases

40Ar/39Ar ages point to an initial shield building phase between >1,311 and 1,000 ka (Esser et al., 2004). This would have originally been submarine, with the extrusion of basanitic pillow lavas and

associated submarine pyroclastic rocks. This is in agreement with basanitic hyaloclastites (sub-aqueous or sub-glacial pyroclastic breccia deposits) from the DVDP drilling project at Hut Point Peninsula returning K-Ar ages of 1,340 ± 230 ka, indicating the earliest Erebus activity (Kyle, 1981). The transition from sub-aqueous to sub-aerial activity is in the form of a highly fractured and weathered tephritic dike intruding other volcanic deposits at Cape Barne, dated at 1,311±16 ka (Moore & Kyle, 1987).

Proto-Erebus cone building is the second phase proposed by Esser et al. (2004), occurring between ~1000-250 ka. Basanite/tephritic activity evolved to more differentiated lavas of phonotephrite and tephriphonolite composition between 1,250 and 890ka. The increase in silica of these more evolved lavas lead to viscosity increases and steeper slopes, forming a cone referred to as Proto-Erebus, with slopes in excess of 35˚; these slopes contrast with the slopes of phase 1 activity at around 9˚, clearly visible in the slope map as a slope break (Figure 3). Fang Ridge, a 7km long escarpment to the north of the modern Mt Erebus summit, and also visible in both Figure 2 and 3, is interpreted to be the sole remnant of Proto-Erebus, although the disappearance of the remainder of the cone still presents challenges. Two theories are proposed: 1) sector collapse to the south-west, with long run-out distances displacing and hiding the collapse evidence in McMurdo Sound, and 2) subsidence and the formation of an associated caldera through 'passive' magma removal (rather than catastrophic evacuation, due to the lack of pyroclastic deposits from such an event). Passive removal generally results from the eruption at non-summit vents, although the lack of parasitic cones raises questions on the validity of this interpretation. The subsidence and formation of the modern Erebus (Harpel et al., 2004), leads to believe that the same may have happened to Proto-Erebus.

Phase 3 of the Erebus volcanic evolution is a modern Erebus cone building period (Esser et al., 2004). Anorthoclase-phyric eruptions began at around 250 ka, similar to the anorthoclase-phyric younger lavas, and probably marks the transition between Proto-Erebus and modern Erebus. The summit vent developed around 2km south-west of the estimated Proto-Erebus summit vent, based on the morphology of Fang Ridge (Figure 3). Between 250 and 90 ka, there was a significant increase in volcanic activity, probably building the majority of the modern Erebus cone, seen as long (up to 5km) and wide (up to 50m) flows and flow levees of tephriphonolitic composition on the steep upper slopes. The most recent of these effusions are truncated by an escarpment containing an 87±14 ka lava flow, representing the end of the high activity period of phase 3.

The chemical evolution of Mt Erebus is summarised in Figure 4 from Esser et al. (2004, and references therein). Younger rocks are generally more evolved, with a greater silica and alkali content.

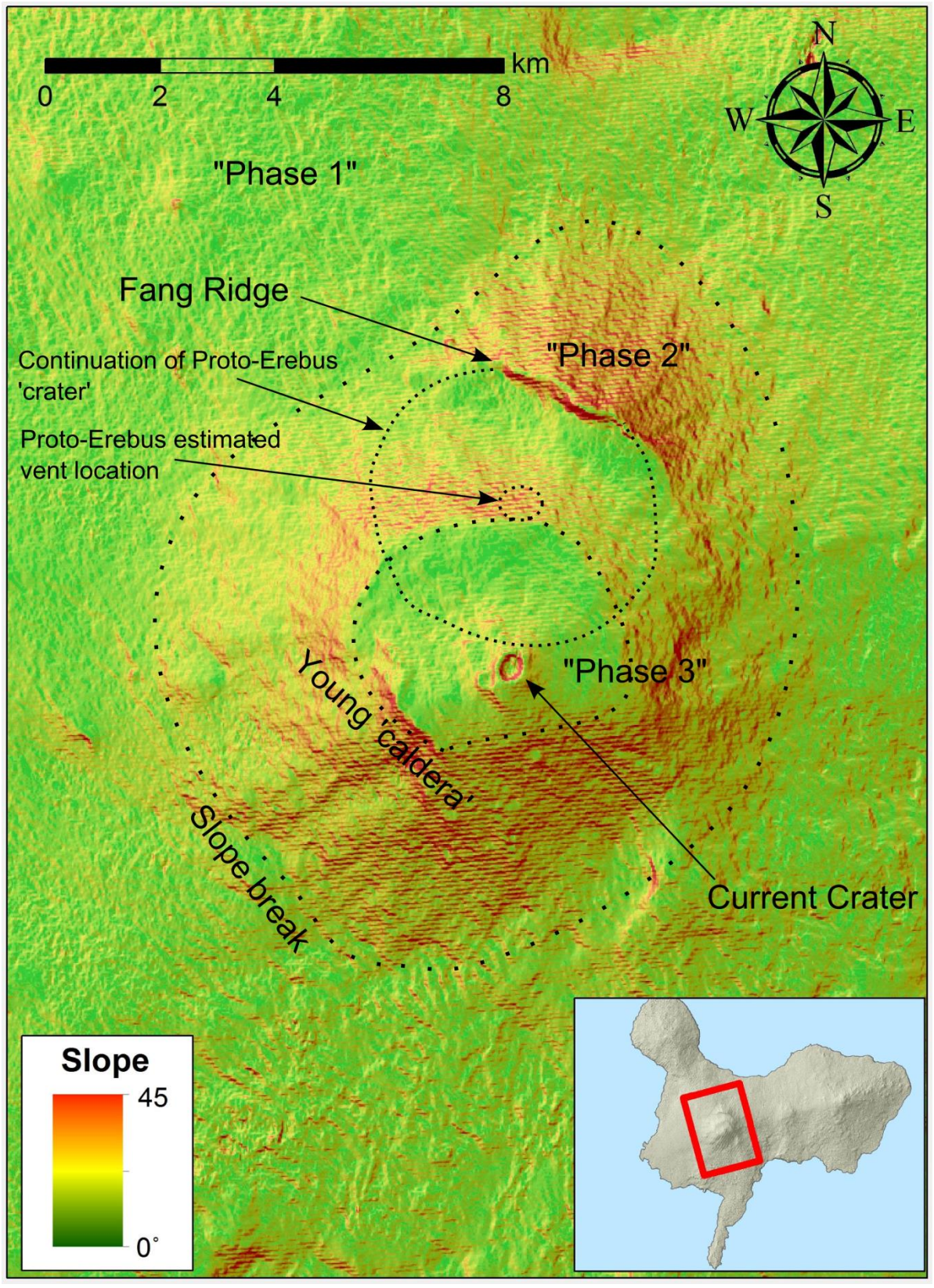

Figure 3. Slope map of Mt Erebus highlighting the differences in slope between the phase 1 and phase 2/3 volcanic activity periods proposed by Esser et al. (2004). Red areas represent steeper slopes, while green represents shallow slopes. The slope break shows a major difference between younger 35˚ slopes and the older 9˚ slopes of the lower shield. The inset map indicates the extent of the main map in relation to Ross Island. A crater boundary and vent location of Proto-Erebus is estimated based on the morphology of Fang Ridge.

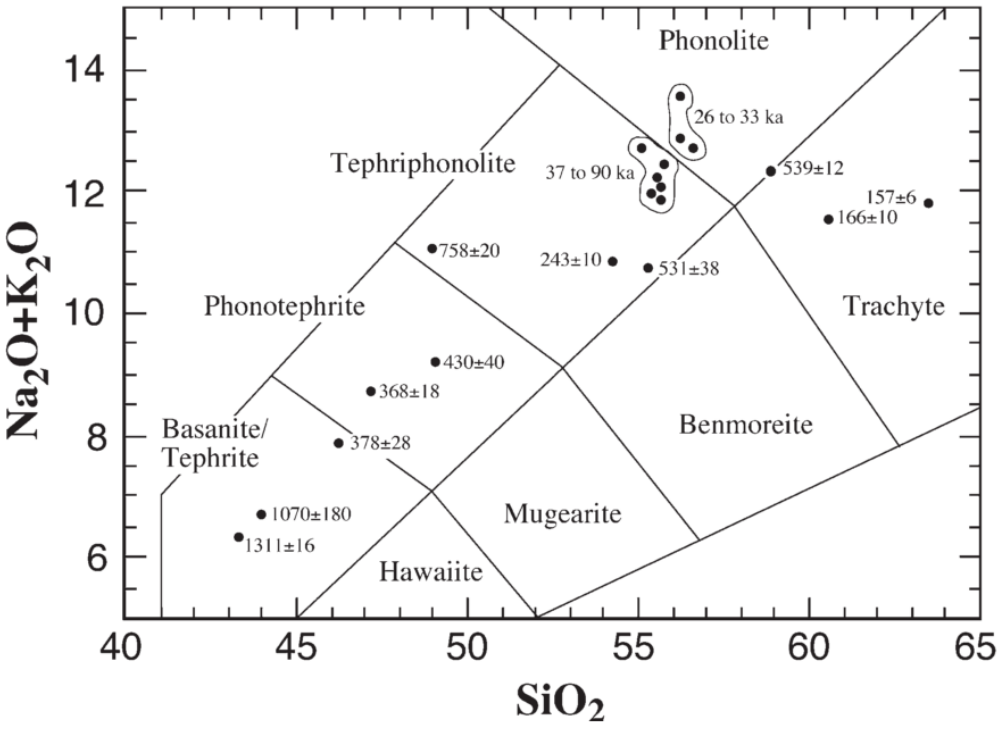

Figure 4. BAS diagram showing the chemical evolution of Mt Erebus volcanic products. Older rocks are generally more primitive (Basanite/tephrite), while younger more evolved rocks have high silica and alkali contents (tephriphonolite/phonolite). From Esser et al. (2004), produced from data from Kyle et al. (1992). Compositional boundaries from Le Bas, Le Maitre, Streckeisen, & Zanettin (1986)

Historical Activity

The volcanic history of Erebus is very limited, as it was only discovered in 1841 by James Clark Ross and his crew about the ships *Erebus* and *Terror*. Ross conducted the first geological observations for Erebus, stating that:

> *"…Mt Erebus was observed to emit smoke and flame in unusual quantities, producing a most grand spectacle. A volume of dense smoke was projected at each successive jet with great force, in a vertical column, to the height of between fifteen hundred and two thousand feet above the mouth of the crater… whenever the smoke cleared away, the bright red flame that filled the mouth of the crater was clearly perceptible; and some of the officers believed they could see streams of lava pouring down its sides until lost beneath the snow…"* (Ross, 1847, p.220-221)

After the discovery by Ross, observations of the activity is limited to occasional sightings up until the 1970s when regular detailed recordings begun (Harpel et al., 2008). The first ascent in 1908 observed three well-like openings in the summit crater along with intermittent roaring noises (David & Priestley, 1909). Later that year, further steam eruptions were observed and in June, strong outbursts of steam and ash, and evidence for molten lava in the crater were observed by the red glow that lit up the plume.

David and his crew made a second ascent in 1912, during which an explosive eruption occurred emitting blocks of pumiceous lava, containing pele's hair (Priestley, 1913). Observations are lacking until 1924, when no significant activity was recorded, although in January 1935 a plume of steam was observed (Berninghausen & van Padang, 1960).

Observers in an aircraft reported an orange glow in 1957 and 1958 (Giggenbach et al., 1973), and a 1967 aerial survey recorded high temperatures, although measurements were not provided (Burge & Parker, 1967). Photos from 1972 show dark ash in the main crater floor, indicating continued intermittent explosive activity (Giggenbach et al., 1973).

Since these records, observations have increased significantly, and a volcanic monitoring network has been set up, run through the Mt Erebus Volcano Observatory (MEVO, http://erebus.nmt.edu/) at the New Mexico Institute of Mining and Technology (NMIMT). During the summer, MEVO run a webcam with 'live' imagery being uploaded periodically, and all year round have 13 seismic sensors of varying types operating (4x short period, 7x broadband, 2x infrasound). The combination of video (including acoustic) and seismic recordings have allowed for a highly detailed account of each eruption, including flight times of bombs within the crater, magnitude, vent location, and details about the ash content of the eruption (Dibble, Kyle, & Rowe, 2008; Rowe, Aster, Kyle, Dibble, & Schlue, 2000).

Mt Erebus has shown enhanced explosive activity only twice in more than 35 years. In 1984, sustained strombolian eruption ejected bombs up to 10m in diameter up to 2km from the vent and sending small eruption columns up to 2km into the air, and in 1993 two phreatic explosions created a small crater in main summit crater (Caldwell & Kyle, 1994; Dibble, Kyle, & Skov, 1994; Kyle, 1990)

During observations between 1986 - 1990, seismic activity ranged from 1-184 events per day, with up to 4 eruptions per day and persistent degassing (Dibble et al., 2008). The eruptions were strombolian in type, resulting from a single coalesced bubble rising to the surface (some up to 35m in diameter) and exploding from the convecting lava lake. An example of such an eruption can be seen in the thermal imagery of Figure 5 below.

Six years (Jan 2001 – Dec 2006) of satellite observations over Erebus (NASA's Moderate Resolution Imaging Spectroradiometer, MODIS) shows a variable radiant flux over the time scales of days to weeks, although little variation over an inter-annual period (Wright & Pilger, 2008). This contrasts greatly with other long term 'stable' lava lakes around the world, which had much greater variation in radiant flux. Higher fluxes (100MW) occurred during periods of greater activity. Infrared monitoring of lave lake activity from the crater rim shows a pulsatory behaviour with a period of 12 minutes, punctuated by a sudden spike in activity during bubble release.

Explosive Eruptions Producing Tephra

As this analysis of volcanic hazards is based largely on ash fall, it is imperative that previous studies of tephra accumulations are considered.

A study on the geology surrounding the side crater of Erebus (the non-active portion) identified a pyroclastic deposit >10m thick (Panter & Winter, 2008). Bombs ranged from 10cm to 4m and increased in number towards the top of the deposit. It is interpreted to be the result of an explosive event with rapid pulsing of strombolian and phreatomagmatic behaviour, with the input of water (likely from a shallow geothermal source) reducing towards the end of the eruption, leading to reduced fragmentation and a greater quantity of bombs being ejected. While the tephra was only located around the south-western rim, it is suggested by Panter & Winter to have been much more extensive, and to have extended down the slopes at least until the accumulation area of the Barne Glacier, the focus of the following study.

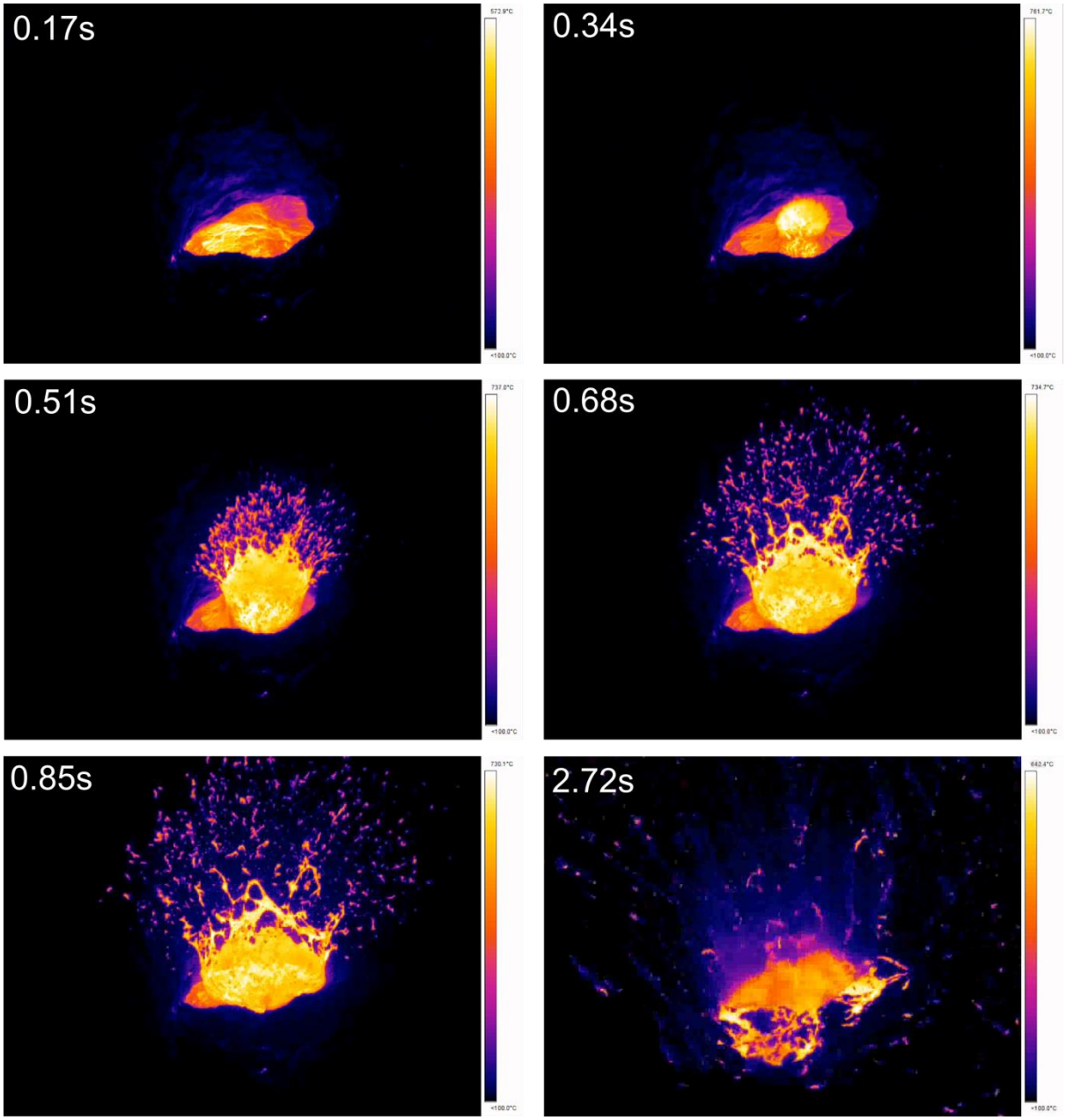

Figure 5.FLIR Infrared imagery from an eruption in 2012 showing a single strombolian eruption from the lava lake in the main crater of Mt Erebus. The lava lake is roughly 30m across, and the FLIR camera is ~300m from the lake. Frame rate roughly 6/sec, leading to 0.17sec frames. From Peters, Oppenheimer, & Kyle, (2014).

Englacial Tephrostratigraphy

Dating of englacial tephra appears to be the most successful method for explosive eruption analysis, such as was done in the studies Harpel et al. (2004) and Harpel et al. (2008). Three englacial tephras have been dated at the terminus of Barne Glacier (west flank of Erebus, terminating south of Cape Barne and Royds), giving ages of 71 (±5, EBT-2), 39 (±6, BIT-272), and 15 ka (±4, EBT-63; Harpel et al., 2004). The zone of accumulation for the Barne Glacier is not well defined, although had the tephra been deposited in the estimated accumulation zone 10-15km upslope from the terminus, this would still indicate an aerial transport distance of 7-12km from the modern day vent. Tephra thickness would allow for plume models to be developed and would assist in this projects hazard modelling, however due to the englacial nature of the deposit, it is likely to have been deformed and may not

accurately show the true thickness. The ice containing the youngest tephra layer (15±4 ka), was found to have 19 up-slope tephras, and as the ice was undeformed it implies that at least 19 tephra producing events have occurred and deposited material to the western flank since the 15 ka eruption event, while the 71 ±5 ka tephra predates at least 5 more layers. Harpel et al. (2008) goes on to identify a total of 43 eruptions of varying sizes, formed through a combination of strombolian and phreatomagmatic eruptions. Few were identified to have solely originated from strombolian activity.

Two distal englacial tephra deposit interpreted to have originated from Mt Erebus have been identified. The first is a plinian tephra which has a phreatomagmatic component, and was dated by Harpel et al. (2004) at an age of 39±6 ka and may have been associated with the first of the two proposed modern Erebus caldera forming events mentioned earlier. It was recovered in the Mt DeWitt area, ~180km west of Erebus. The second is an undated phreatomagmatic tephra from the Manhaul Bay area, around 200km north-west of Erebus, but is presumed to be <36 ka based on chemical composition (Harpel et al., 2008).

The evidence seen in these studies indicates that Erebus has had a much more active past than historically observed, with ash fall reaching distances that are likely to have great impact on anthropogenic activities.

Wind

The winds around Ross Island and the Ross Ice Shelf are complex, due to many topographical and climatological conditions. Katabatic winds from the south extend out across the Ross Ice Shelf where they interact with major landforms, such as Ross Island.

By far the most common wind direction at Scott Base is from the north-east (Figure 6). The windrose below was created using data from the "Ant Scott Base AWS" weather station during the period of the 13th December 1996 and the 12th September 2010.

The wind around the summit of Erebus, almost 4000m above the surrounding ocean and ice shelf, is observed to experience different wind regimes. This is often noticed when an observer at sea level experiences a wind direction that is inconsistent with the direction of the plume emanating from the summit of Erebus. The prevailing all-year round wind at the summit is west-southwest, while summer winds are more often from the south or south-east (Keys, 1980). The observers' location on the upper slopes will have a great influence on the measured wind speed and direction, although winds approaching the slopes of Erebus are generally observed to travel parallel to contours, rather than ascending or descending.

The complexity of the wind regimes and the lack of detailed recordings of atmospheric winds in the 0 – 10km range make volcanic modeling difficult. Where data is available, it is often restricted to summer months or over short time scales, that may not be representative of the longer term average. For example the long term average of 14 years of recordings surficial recordings at Scott Base ground level (Table 1) differed significantly from the observed short term wind regimes by Keys (1980) during one month of recordings.

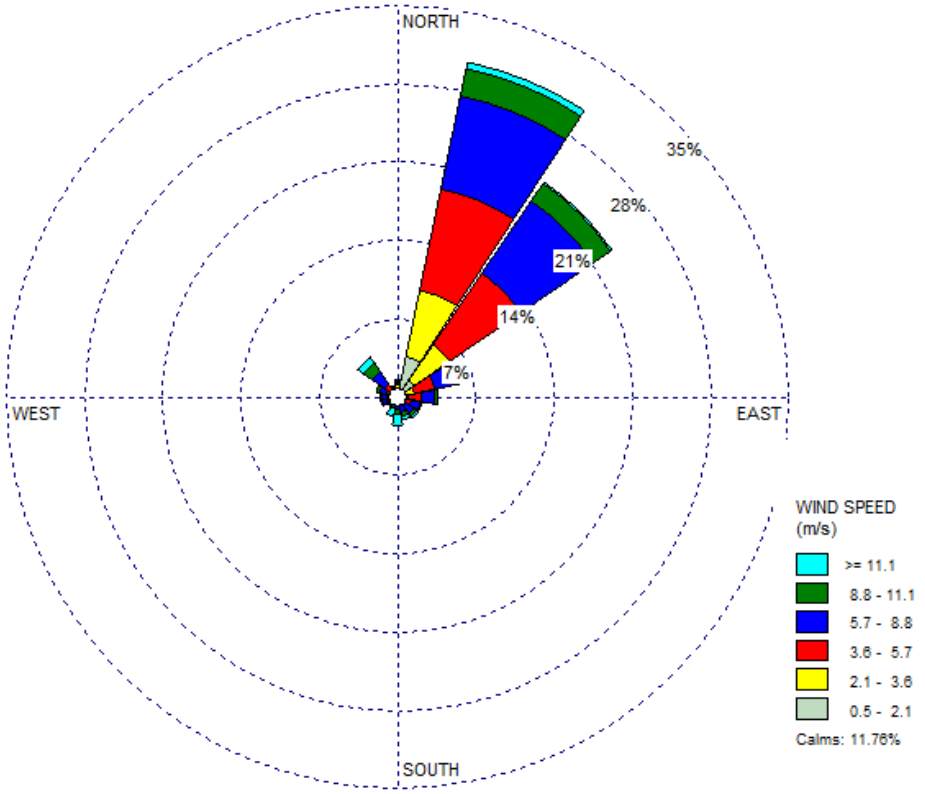

Figure 6. A windrose for the 3-hourly wind conditions observed at Scott Base (weather station: Ant Scott Base Ews, #12740) during the period 13th December 1996 to 12th September 2010. Data taken from the CliFlo database (NIWA, 2014).

Table 1. Frequency (%) of wind directions at Scott Base and above Erebus summit campsite (1972-79). Above ground observations are from Keys (1980) between the period November 1972 – December 1979. Surface measurements from NIWA's CliFlo over the period 1996-2010, and have been normalised to ignore calm days (11%; NIWA, 2014).

Wind Direction	Surface (Scott Base)	2700m	3600m (Erebus Camp)	5100m
North	59	27	7	41
East	21	11	32	4
South	9	35	50	15
West	9	27	11	40

Methods

This method section is designed so that the hazard mapping techniques used here may be replicated through other volcanoes around the world, and therefore is considered more of an instructional 'how to do' rather than 'what we did'.

This method involves GIS techniques used to determine stream flow paths and catchment areas and can go on to determine the volume of rain that has fallen upstream of a certain point (assuming no evaporation or loss to groundwater). In the case of volcanic hazards, the method can substitute out rainfall volume and use the volume of erupted material which can be used as a proxy for debris flow potential.

The full methods process has been summarised as a flow chart in Figure 8 below.

The 1:50k contours (LINZ, 2014) were first made into a DEM[2], which was then clipped to the Ross Island area[3]. The Ross-Ice shelf was ignored for flow mapping, due to its extremely low gradient.

Developing a Flow Accumulation Map

The flow accumulation map was generated to determine the flow paths that exist on the slopes of Erebus, which can be further used to verify predicted debris flow paths when coupled with tephra thicknesses. Flow accumulation works by first assigning each cell a flow direction[4], based on the value of that cell (high value cells (eg. those with high elevation) flow into lower value cells (eg. those with lower elevation)), before determining the number of cells that flow into a reference cell. For each cell that exists upstream of a reference cell, the value of the reference cell will increase by 1. In Figure 7 below, the highest value cell indicates that it has 35 cells upstream, while cells with a value of zero have no cells flowing into them.

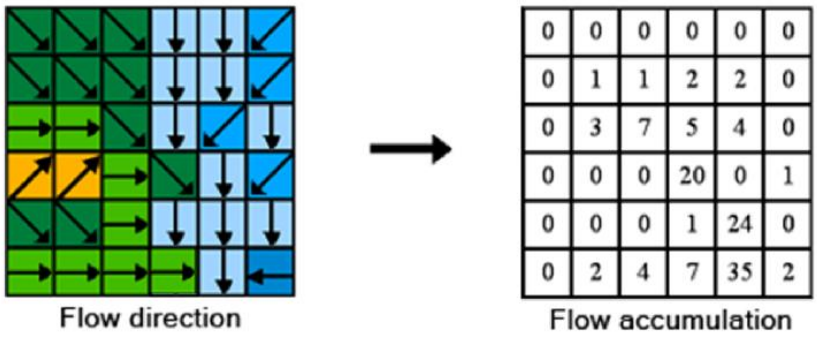

Figure 7. An example of the flow direction and flow accumulation process. REFERENCE (ARCMAP http://help.arcgis.com/en/arcgisdesktop/10.0/help/index.html#//009z00000062000000.htm)

When cell size is known, the value of a flow accumulation cell can be converted to an area value representing the area of the upstream catchment, using the following formula:

$$(Area\ of\ one\ cell) \times (Number\ of\ cells) = Upstream\ Catchment\ Area$$

[2] ArcToolbox > Spatial Analyst > Interpolation > Topo to Raster
[3] ArcToolbox > Data Management > Raster > Raster Processing > Clip
[4] ArcToolbox > Spatial Analyst > Hydrology > Flow Direction

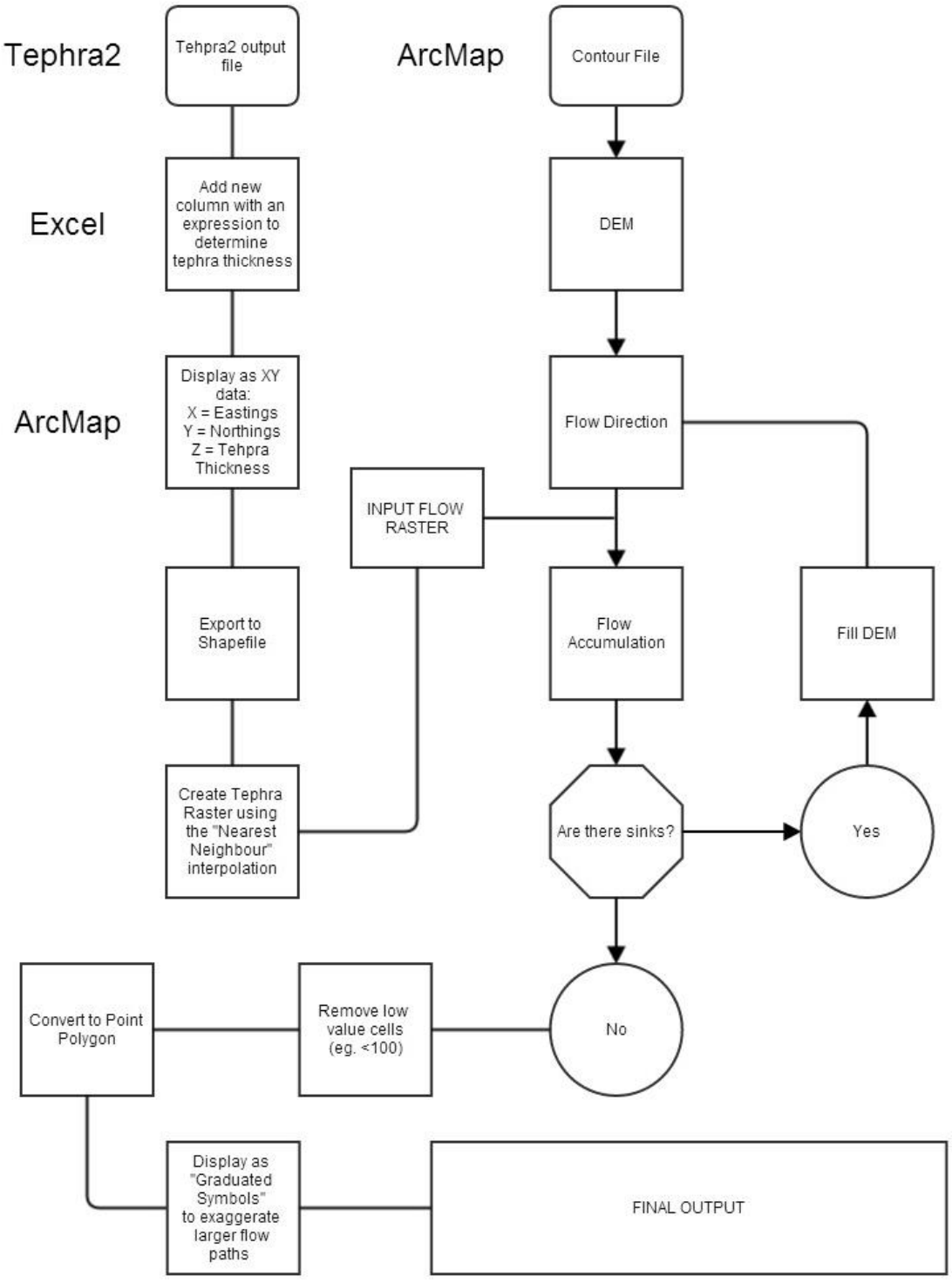

Figure 8. Flow chart describing the methods used in this study.

Sinks

Major limitations of the DEM, along with all hydrological models, are 'sinks' within the data. Sinks are cells (or a series of cells) through which a flow direction cannot be assigned to one of the surrounding 8 cells. This occurs in two situations: 1) when the surrounding cells are of higher values than the processing cell, or 2) when two cells flow into each other. Figure 9 shows an example of a

flow accumulation[5] map in which sinks have not been corrected for. The major tributary, running from the left to the right) reaches a cell lower than the surrounding 8 cells and is nullified, misrepresenting the flow accumulation downslope. This particular tributary represents a catchment area of 7.1km^2 (14,218 cells @ 500m^2/cell).

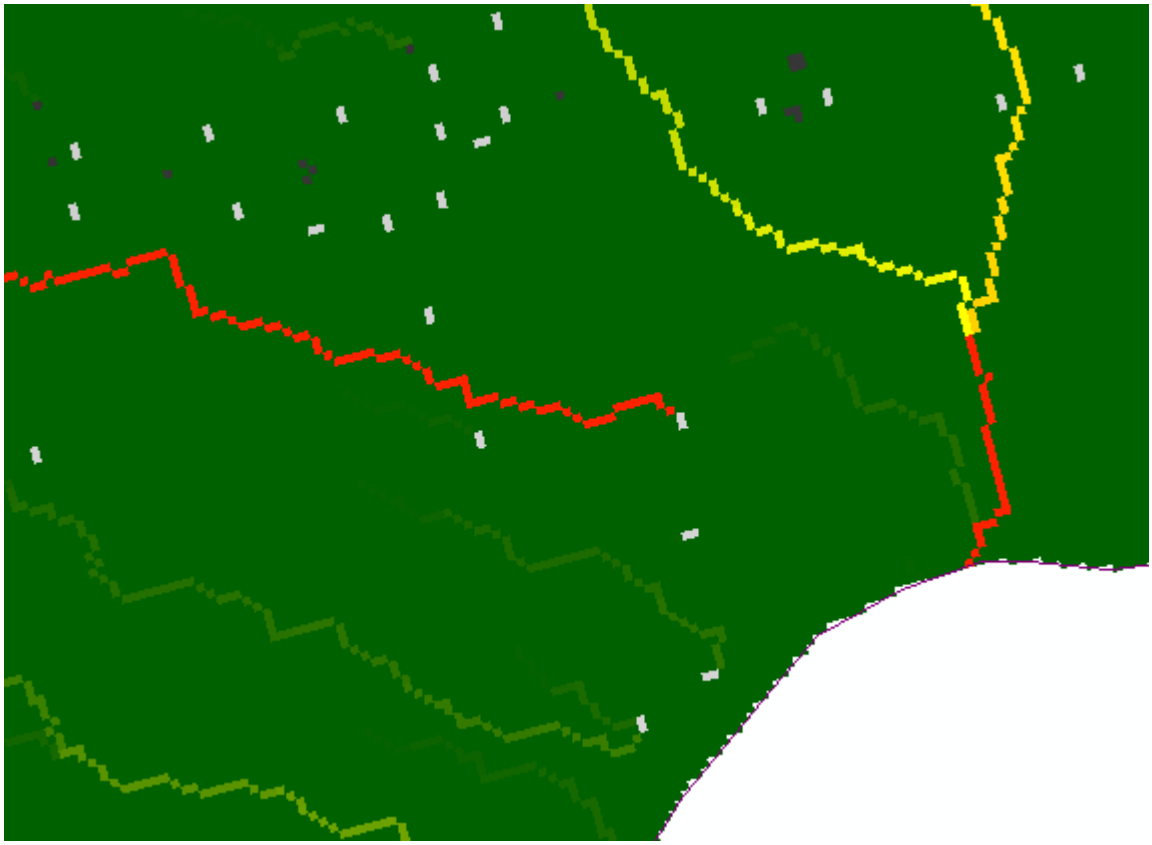

Figure 7. An example of a flow accumulation path reaching a sink and becoming nullified. This particular flow accumulation path (running from left to right) represents the catchment area of 7.11km^2. They light and dark grey represent other sinks in the data. The field of view here

ArcMap's 'Sink' function[6] was run and determined 26,469 sinks in the Ross Island clipped DEM. To develop a sinkless DEM, otherwise known as a depressionless DEM, the 'Fill' function[7] was used. From here, a flow direction, followed by a flow accumulation map was recreated to show flow paths based on Ross Island topography (Figure 10). The flow accumulation map represents a catchment map, and can be manipulated to show catchments based on catchment areas above a certain value (ie. greater than 10km^2).

There are a total of 50 catchments greater than 10km^2 on Ross Island, based on flow accumulation calculations. Table 2 sums up the distribution of catchment areas, many of which exist as a single unit at the resolution of the DEM along the coast. Unsurprisingly, the largest catchments mirror glacial paths and outlets, including the Barne (55 km^2), Erebus (55 km^2), Terror (90 km^2), and Aurora (123 km^2) glaciers (Figure 8). The largest catchments are also focused on the south and south-west coasts of Ross Island.

[5] ArcToolbox > Spatial Analyst > Hydrology > Flow Accumulation
[6] ArcToolbox > Spatial Analyst > Hydrology > Sinks
[7] ArcToolbox > Spatial Analyst > Hydrology > Fill

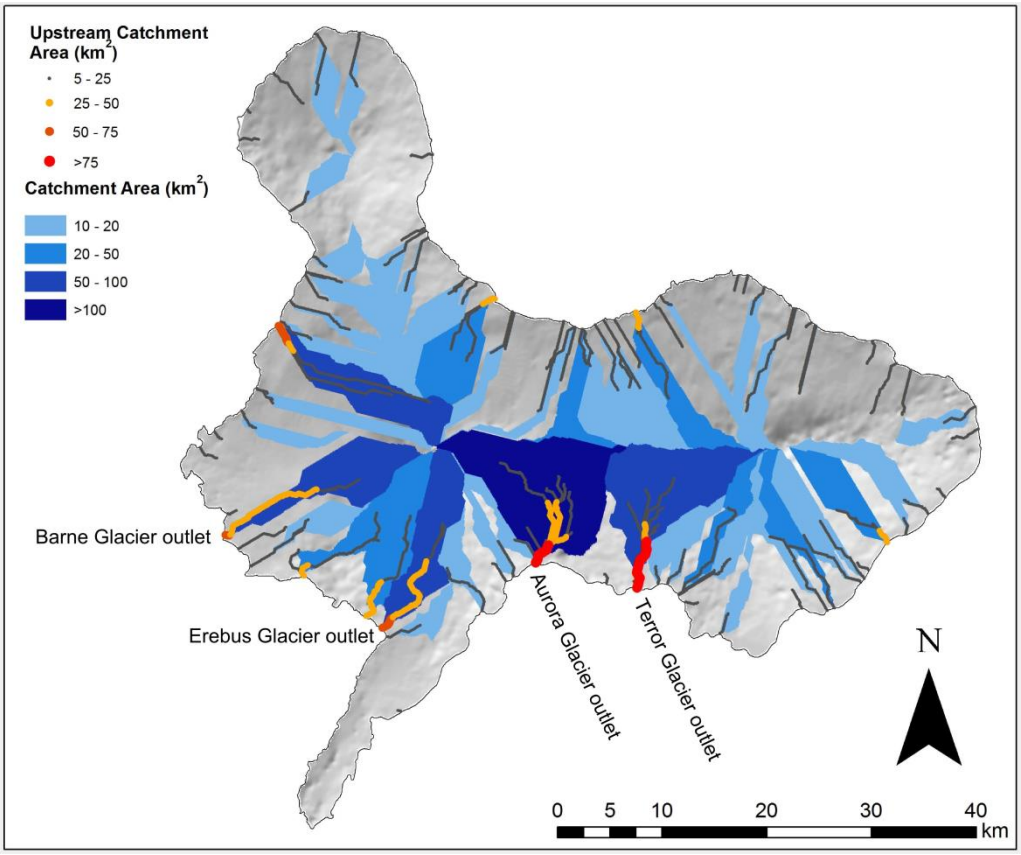

Figure 8. Catchments of Ross Island that are >10km2. Grey-lines represent a flow path with >1km^2 upstream. Green coloured areas represent catchment areas >10km^2.

Table 2. A summary of the catchment areas of Ross Island. The total number of catchments is high (14766) as DEM cells at the edge of the island may constitute a single celled catchment.

Catchment Area (km^2)	# of catchments
>0 (any size)	3983
>1	289
>10	50
>50	5
>100	1

Tephra Isopachs

Numerical models of tephra hazard assessments can be grouped into two categories: particle tracking models, and advection-diffusion models. Particle tracking models are Eularian or Langrangian models and are used to forecast the position of the volcanic ejecta in the atmosphere at a given time, and are specifically useful for airlines to predict ash cloud movements. Advection diffusion models are Eularian models that forecast tephra accumulation on the ground surface in relation to the eruption source.

Tephra2 (Bonadonna, Connor, Connor, & Courtland, 2013) is advection-diffusion modeling software. The model requires information on eruption parameters, particle parameters, atmospheric parameters, and grid parameters, as follows:

- **Eruption parameters**
    - Volcano location (UTM easting and northing)

    - Elevation (m)
    - Mass erupted (kg)
    - Particle size distribution (phi)
    - Plume height (m)
    - Integration steps
- **Particle parameters**
    - Fall time threshold (s)
    - Diffusion coefficient (m/s)
    - Lithic and pumice densities (kg/m^3)
    - Integration steps
    - Plume dispersion model
- **Atmospheric parameters**
    - Atmosphere levels (m)
    - Wind speed (m/s)
    - Wind directions (degrees)
- **Fallout (grid) parameters**
    - Grid point locations (UTM)
    - Elevation (m)

Full information about the equation and calculation steps can be found in the Tephra2 Users Manual (Connor, Connor, & Courtland, 2011).

Creation of Contours from Tephra2 Output File

The resulting Tephra2 output contains both grid and contour files containing data on mass per unit area and weight% of each phi size. The output text file (.txt) is in the following format:

Easting Northing Elevation Mass Wt_%_Min_Phi Wt_%_Min_Phi

As example of which is as follows:

531790 1382690 400 8.8 17 30 31 19 3.4 0.074 0.00012 1.8e-09
531790 1383190 400 0.77 29 27 24 17 3.7 0.098 0.00018 2.9e-09
531790 1383690 400 0.1 58 31 7.1 2.9 0.91 0.043 0.00012 2.5e-09
531790 1384190 400 0.025 55 37 7.5 0.81 0.053 0.0058 3e-05 9.7e-10
531790 1384690 400 0.0045 45 42 11 1.6 0.0062 0.00058 7e-06 4e-10
531790 1385190 400 0.0006 33 46 18 3.8 0.016 4.8e-05 1.5e-06 1.8e-10

Tephra2 calculates values for each of the grid point provided (Figure XX), however it does not provide a thickness of tephra deposits. This can be derived using the density and the mass per unit area. As the area for the mass per unit area is $1m^2$, this value can simply be divided by the density to determine the tephra thickness (in metres) for that unit area ($1m^2$). A further division provides values in cm.

$$Tephra\ thickness\ = \frac{Mass\ per\ unit\ area}{Density}$$

Using the easting, northing, and the recently derived tephra thickness values, these can be plotted as a classified raster[8] followed by a contour plot[9] in ArcMap (Figure 11 below).

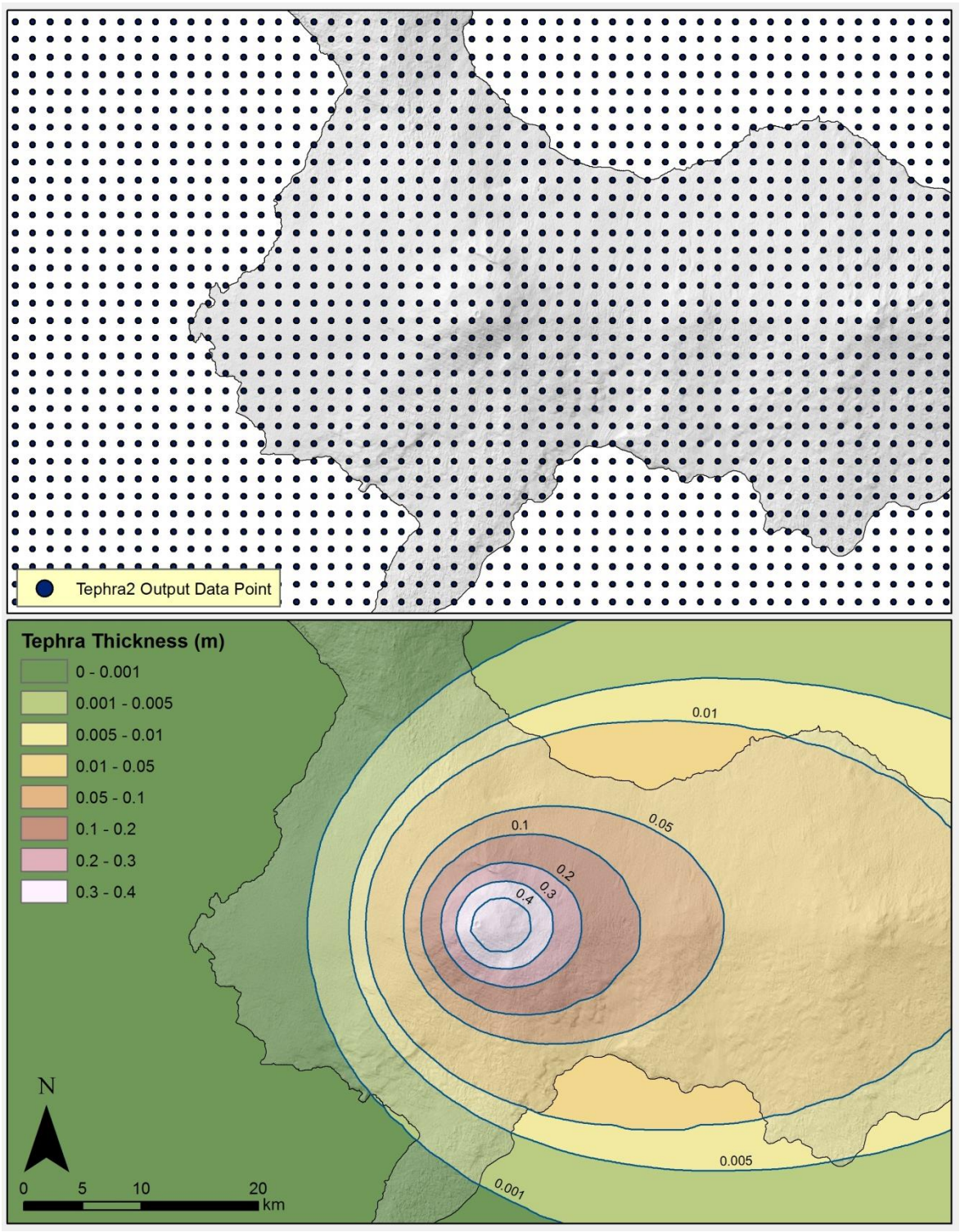

Figure 9. Top: An example of the output grid file generated by Tephra 2. Bottom: An example of a graduated raster (coloured) and contour plot (blue lines) derived from the Tephra2 output file. Contour values are in metres. This

[8] ArcToolbox > Spatial Analyst > Interpolation > Natural Neighbour
[9] ArcToolbox > Spatial Analyst > Surface > Contour List

example shows a plinian eruption with an eruption column of 20km and an eruption mass of $1x10^{11}$ kg. The eruption plume is affected by a westerly wind.

While Erebus has been identified as being responsible for two plinian eruptions in the past 40ka, distributing ash as far as 200km away from the vent (Harpel et al., 2008, 2004), this study models a more likely strombolian type eruption. Little data is available on single eruption events, such as estimated eruption column height or ejected volume, mostly in part to the geological mapping challenges mentioned earlier, and also the englacial nature of tephra outcrops preventing the recording of tephra thickness and distance from source as they may be been transformed and transported.

The parameters were estimated as follows:

Table 3. Parameters used for the modelling of a strombolian eruption in Tephra2.

Plume Height	7000 m
Eruption Mass	$1x10^{10}$ kg
Max Grainsize	-5 phi
Min Grainsize	5 phi
Median Grainsize	-1 phi
STD Grainsize	2 phi
Vent Easting	552127.016
Vent Northing	-8606706.408
Vent Elevation	3700 m
Eddy Constant	0.04
Diffusion Coefficient	1000 m/s
Fall Time Threshold	100000s
Lithic Density	1000 kg/m3
Pumice Density	1000 kg/m3
Column Steps	100
Plume Model	0
Plume Ratio	0.1

The majority of these values are derived based on parameters used for similar sized strombolian events, provided in the Tephra2 User's Manual (Connor et al., 2011). The results are validated using data from (Harpel et al., 2008), who identified 43 englacial tephra layers which are expected to have been deposited in the upper catchment of the Barne Glacier, 7-12km from the vent.

Debris Flow Mapping

The debris flow map is built by creating a flow accumulation map using a flow direction file (as shown earlier) and weighting it with the tephra thickness output from Tehpra2. The resulting flow accumulation dataset indicates the catchment volume of the erupted ash, and acts as a proxy for debris flow potential post eruption. Larger catchments are likely to contain more ash volume, but this is amplified as distance to the vent decreases.

$$Area\ of\ one\ cell\ (m^2) \times total\ tephra\ thickness\ (m) = Catchment\ tephra\ volume\ (m^3)$$

The data was then clipped to the Ross Island coastline, and the low insignificant values from the tephra flow accumulation data were purged using a Raster Calculator[10] and the following function:

$$SetNull(\text{"RasterLayer"} < \text{"Value"}, \text{"RasterLayer"})$$

"RasterLayer" refers to the layers being purged, while "Value" refers to the value below which values within "RasterLayer" should be deleted. For display purposes the now purged tephra flow accumulation layer was converted to a point shapefile[11], and displayed as graduated symbols to show the buildup of eruption volume as streams coalesce.

[10] ArcToolbox > Spatial Analyst > Map Algebra > Raster Calculator
[11] ArcToolbox > Conversion Tools > From Raster > Raster to Point

Results

The following results section shows the Tephra2 outputs and debris flow accumulation maps for three wind scenarios: no wind, weak northerly wind (5m/s), and strong northerly wind (15m/s). These wind regimes are based on the observations from Keys (1980) that winds at 5100m (1300m above the vent) are predominantly northerlies (41%) or westerlies (40%). The northerly wind regime was chosen as it is likely to have the greatest impact on the anthropogenic activities of Scott Base and McMurdo Station to the south.

The eruption parameters are those shown previously in the methods section.

Eruption Scenario 1: No Wind

Figure 12 shows the flow accumulation output map created using a large strombolian eruption with no wind. The three largest catchments contain >50% of the erupted material (Erebus Glacier, Aurora Glacier, Endeavour Piedmont Glacier), with the largest stream containing >22% of all erupted material[12] upstream of its lowest point (Erebus Glacier).

Eruption Scenario 2: Weak Northerly Wind ~5m/s

Figure 13 shows the flow accumulation output map created using a large strombolian eruption with a weak northerly wind (5m/s). The collection of flow paths are dominated by two channels, both reaching the Ross Island coastline near the terminus for the Erebus Glacier. These two flow paths account for 55% of the total ejected volume.

Eruption Scenario 3: Strong Northerly Wind ~15m/s

Figure 14 shows the flow accumulation output map created using a large strombolian eruption with a strong northerly wind (15m/s). The debris flow paths are dominated by the two same channels as with weak northerly wind, the two near the Erebus glacier terminus. This time however, their dominance is even greater; these two flow paths account for 67% of the total ejected volume.

[12] Total ejected volume = 10,000,000 m^3 (0.01km^3)

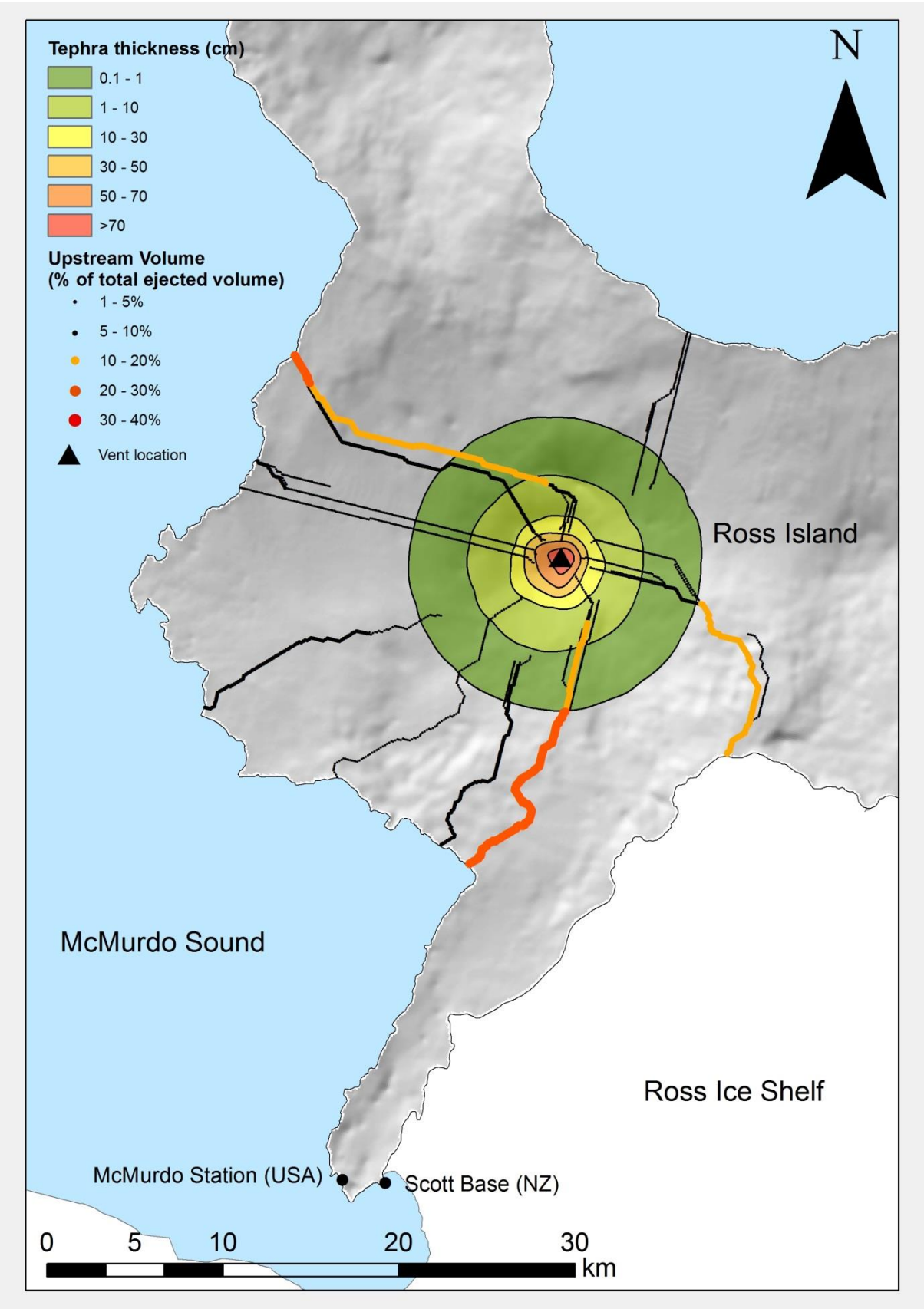

Figure 10. Tephra isopachs and debris flow accumulation map for eruption scenario 1: no wind.

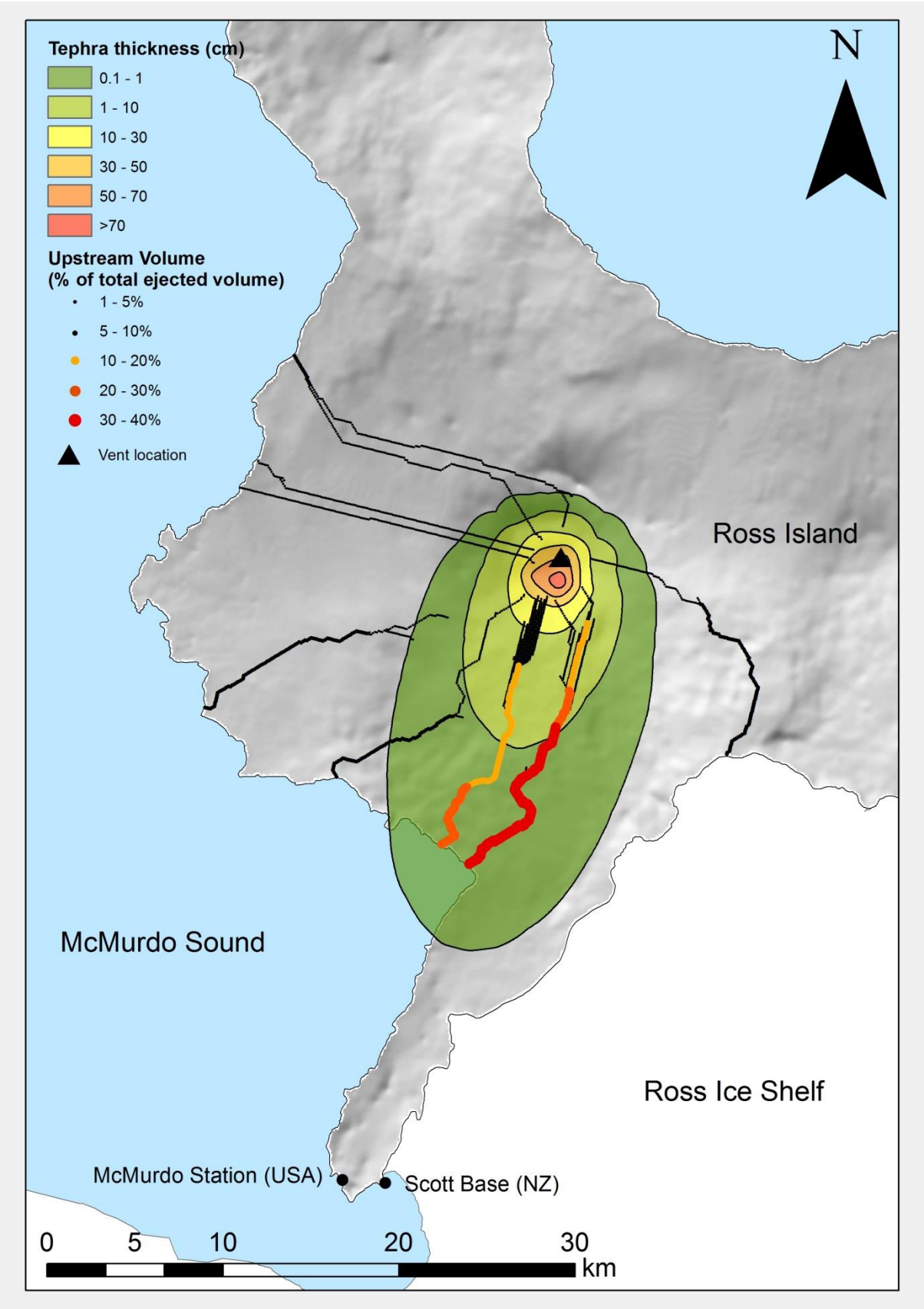

Figure 11. Tephra isopachs and debris flow accumulation map for eruption scenario 2: weak northerly wind (5m/s).

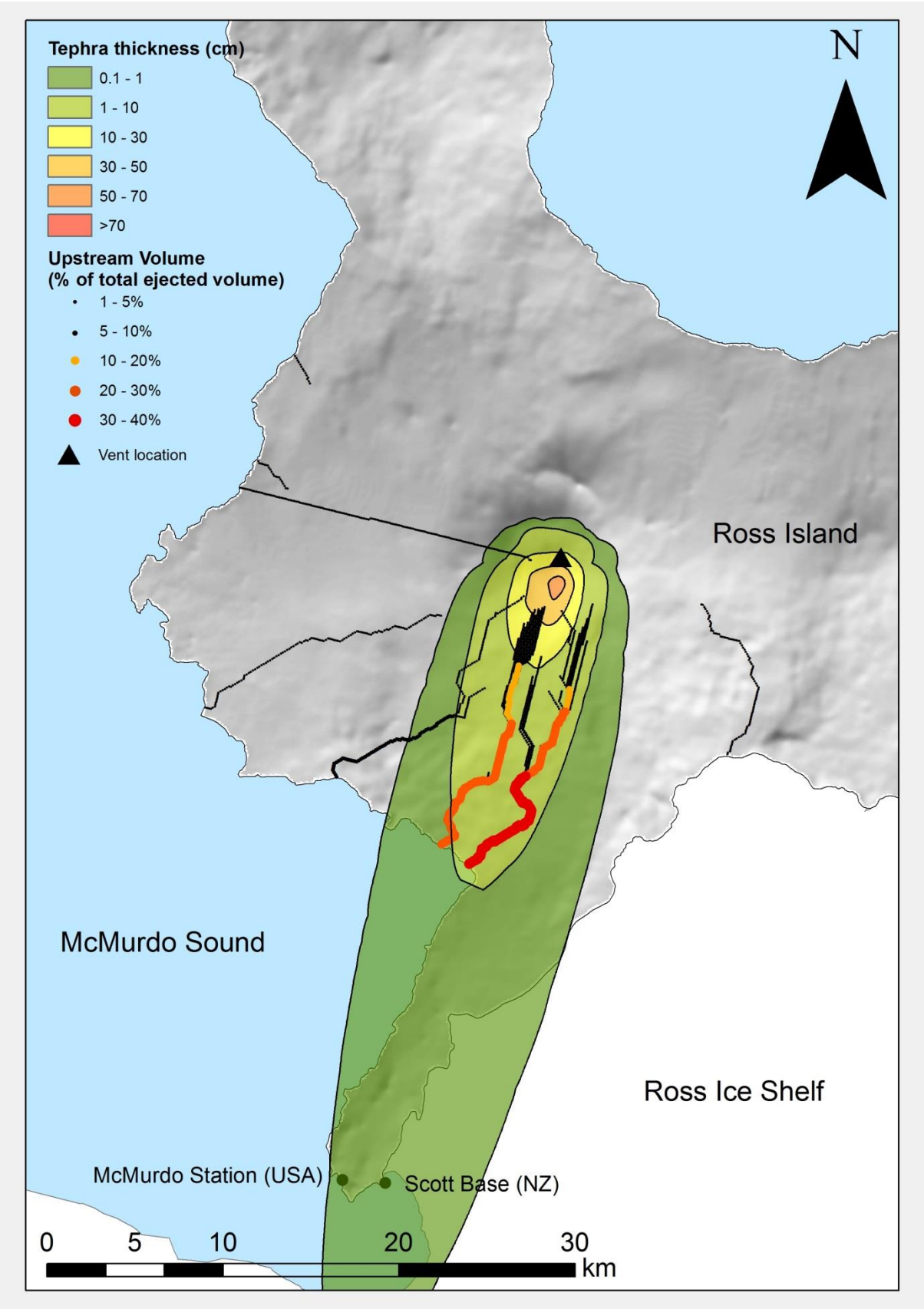

Figure 12. Tephra isopachs and debris flow accumulation map for eruption scenario 2: strong northerly wind (15m/s).

Discussion

Ash fall from these three eruption scenarios only reaches McMurdo Station and Scott Base during optimal wind directions and speeds, and even in the case of the strongest wind, it is on the scale of just over 1mm of deposition. While this may have respiratory implications, the greatest anthropogenic impact will likely be on air traffic and airports as plane engines become damaged when flying through suspended ash (Casadevall, 1994; Dunn, Miatech, & Baran, 1996). If a significant eruption were to occur, dispersal prediction methods would be hampered by the lack of data on atmospheric wind levels.

While the methodology used to create a debris flow map may work well in more central latitudes (with higher precipitation and therefore remobilization potential), the lack of available water and the relationship this will have on the remobilization of ash post-eruption has unknown implications. It is possible that the latent heat of ejecta from the eruption may contribute to snow melt, or the alteration of albedo from the dark ash may aid melting and liquid accumulation to the point where flowing water remobilizes the deposited ash.

In “Scenario 1: No wind”, the Aurora glacier is noted as a major catchment in which ash fall occurs, with almost 20% of the total erupted volume within this catchment (Figure 12). The aurora glacier discharges directly into the Ross Ice Shelf with a transitional slope that gradually decreases until it matches that of the ice shelf. The effect of the extremely low gradient of the Ross Ice Shelf will have unknown effects on a debris flow, other than it will spread out in multiple directions. The accuracy of the DEM limits this prediction.

The accuracies of the catchment areas and flow paths are directly related to the accuracy and resolution of the initial DEM. The resolution of the DEM used in this debris flow accumulation mapping was 100m (derived from 1:50,000 contours at 20m intervals), much lower than that of similar studies, such as Stevens et al. (2002) who used a similar debris flow hazard identification technique on Mt Ruapehu, New Zealand with DEMs of 10m and 20m resolutions.

A DEM of ~23m was available (ASTER Global GDEM V2), and while the resolution was high, the quality of the data was questionable with many sinks identified (the number quoted earlier in the methods section). A comparison between basin and flow path morphology showed that the higher resolution DEM (ASTER) appeared much more natural, while the Topo DEM appeared very linear, something you would not expect in a natural environment (Figure 15).

Future work

There is much potential for further research into the hazards of Erebus, one such area is investigating the modes of wind observed around Erebus. The data is out there somewhere, but is inaccessible and does not appear in peer-reviewed publications.

The geological mapping of Erebus is relatively low compared to other major active volcanic centres around the world. This is in part to the challenges faced by those investigating the geological history of Erebus, although more needs to be done to determine previous explosive events and the magnitude of ash fall; this will aid in tephra hazard mapping.

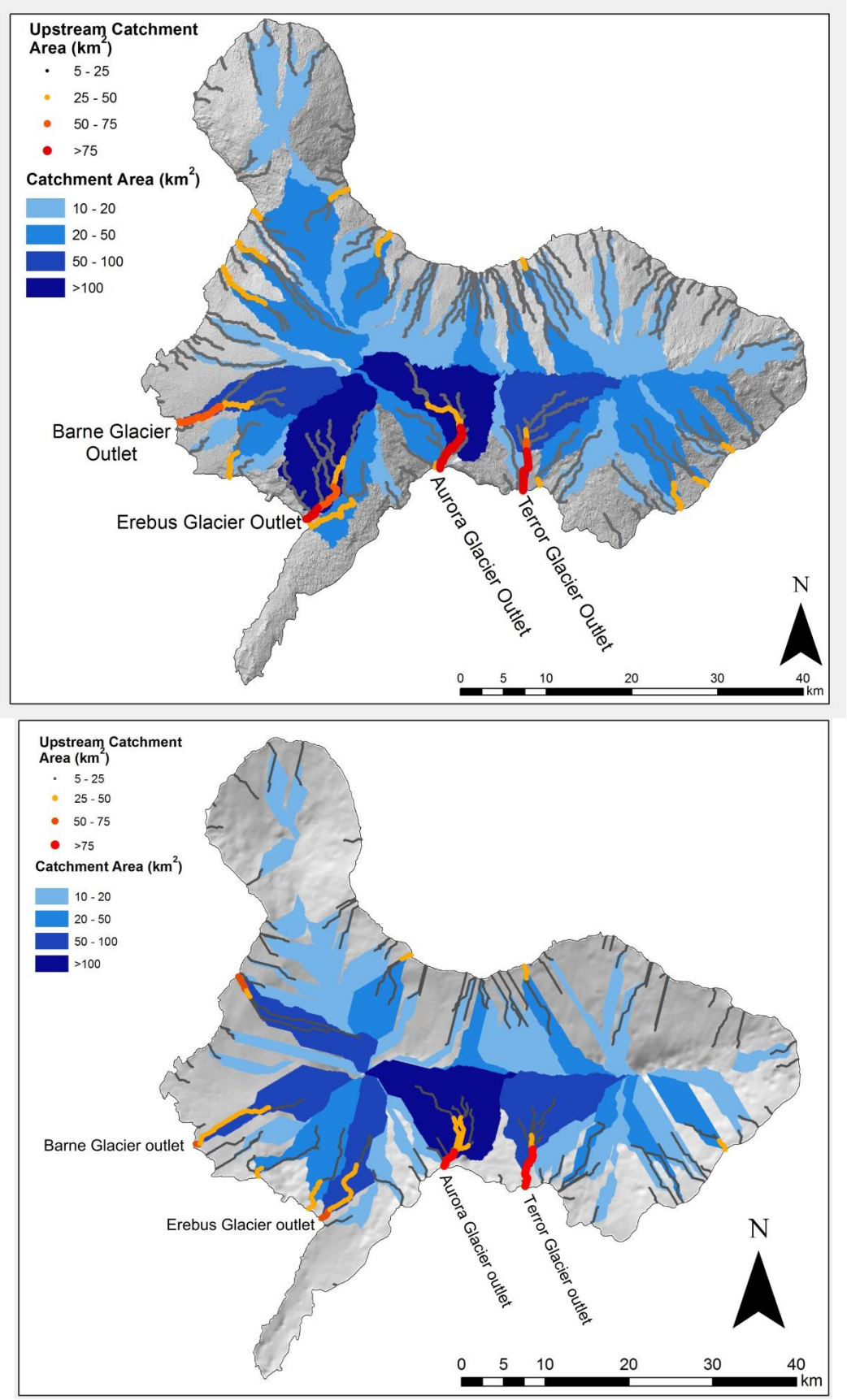

Figure 13. A comparison between the basin and flow accumulation paths in a 23m resolution DEM (top) and a 100m DEM (bottom). The flow paths of the higher resolution map (23m DEM) appear more natural, while those of the lower resolution map (100m DEM) appear more linear.

Conclusion

The article investigates the larger scale hazards of Mt Erebus, an active volcano that makes up the major proportion of Ross Island in the Ross Sea, Antarctica. The volcano has been active since historical records began, although no eruptions of anthropogenic significance have occurred since these records started. Geological evidence is lacking due to high snow and ice cover, harsh environmental conditions and expense of field expeditions, although there is evidence of at least 19 ash producing eruptions in the past 14 ka, that deposited tephra to a distance of at least 7-12km (Harpel et al., 2008, 2004).

Using this geological evidence a strombolian eruption is modeled using the Tephra2 modeling program, which predicts the weight per unit area of ash fall using a set of eruption parameters provided by the user. The eruption appears to have little impact on anthropogenic activities, except for instances of optimal wind (≥15m/s wind speed from the north for an eruption column of 7km and deposition of 1mm at Scott Base and McMurdo).

A flow accumulation map is also modeled in an attempt to determine areas at risk of debris flow hazards, and identifies the major glaciers as the most at risk as they already exist as drainage channels. The major limitation determined by this study is the availability of water to create a debris flow, and it is hypothesized that liquid water may become available from melting by the latent heat of erupted material or the melting effect of albedo alteration from the dark tephra.

References

Berninghausen, W. H., & van Padang, M. N. (1960). *Catalouge of the Active Volcanoes of the World, including Solfatara Fields; Part X, Antarctica* (p. 32). Naples: International Association of Volcanology.

Bonadonna, C., Connor, L. J., Connor, C. B., & Courtland, L. M. (2013, May). Tephra2. Retrieved from https://vhub.org/resources/26

Burge, W., & Parker, D. C. (1967). Infrared Survey in Antarctica. *Antarctic Journal*, *10*(2), 1964.

Caldwell, D. A., & Kyle, P. R. (1994). Mineralogy and geochemistry of ejecta erupted from Mount Erebus, Antarctica, between 1972 and 1986. *Volcanological and Environmental Studies of Mount Erebus, Antarctica*, *66*, 147–162.

Casadevall, T. J. (1994). The 1989–1990 eruption of Redoubt Volcano, Alaska: impacts on aircraft operations. *Journal of Volcanology and Geothermal Research*, *62*(1-4), 301–316. doi:10.1016/0377-0273(94)90038-8

Connor, L. J., Connor, C. B., & Courtland, L. M. (2011). Tephra2 Users Manual. Retrieved from https://vhub.org/resources/756/download/Tephra2_Users_Manual.pdf

David, T. W. E., & Priestley, R. E. (1909). Notes in regard to Mount Erebus. In *The Heart of the Antarctic* (pp. 308–310). London: William Heinemann.

Dibble, R. R., Kyle, P. R., & Rowe, C. a. (2008). Video and seismic observations of Strombolian eruptions at Erebus volcano, Antarctica. *Journal of Volcanology and Geothermal Research*, *177*(3), 619–634. doi:10.1016/j.jvolgeores.2008.07.020

Dibble, R. R., Kyle, P. R., & Skov, M. J. (1994). Volcanic activity and seismicity of Mount Erebus, 1986-1994. *Antarctic Journal of the United States*, *29*, 11–13.

Dunn, M. G., Miatech, J., & Baran, A. J. (1996). Operation of Gas Turbine Engines in Volcanic Ash Clouds. *Journal of Engineering for Gas Turbines and Power*, *118*(4), 724–731.

Esser, R. P., Kyle, P. R., & McIntosh, W. C. (2004). 40Ar/39Ar dating of the eruptive history of Mount Erebus, Antarctica: volcano evolution. *Bulletin of Volcanology*, *66*(8), 671–686. doi:10.1007/s00445-004-0354-x

Giggenbach, W. F., Kyle, P. R., & Lyon, G. L. (1973). Present Volcanic Activity on Mount Erebus, Ross Island, Antarctica. *Geology*, *1*(3), 135–136.

Harpel, C. J., Kyle, P. R., & Dunbar, N. W. (2008). Englacial tephrostratigraphy of Erebus volcano, Antarctica. *Journal of Volcanology and Geothermal Research*, *177*(3), 549–568. doi:10.1016/j.jvolgeores.2008.06.001

Harpel, C. J., Kyle, P. R., Esser, R. P., McIntosh, W. C., & Caldwell, D. a. (2004). 40Ar/39Ar dating of the eruptive history of Mount Erebus, Antarctica: summit flows, tephra, and caldera collapse. *Bulletin of Volcanology*, *66*(8), 687–702. doi:10.1007/s00445-004-0349-7

Harrington, H. J. (1958). Nomenclature of rock units in the Ross Sea region, Antarctica. *Nature*, *182*, 290.

Keys, H. (1980). Air Temperature, Wind, Precipitation and Atmospheric Humidity in the McMurdo Region, Antarctica. In *Antarctic Data Series no. 9*. University of Wellington, No. 17.

Kyle, P. R. (1981). Geological history of Hut Point Peninsula as inferred from DVDP 1, 2, and 3 drillcores and surface mapping. *Antarctic Research Series*, *33*.

Kyle, P. R. (1990). McMurdo Volcanic Group, Western Ross Embayment. In W. LeMasurier & J. W. Thomson (Eds.), *Volcanoes of the Antarctic Plate and Southern Oceans* (Vol. 48., pp. 18–145). Washington, DC.

Kyle, P. R., & Cole, J. W. (1974). Structural Control of Volcanism in the McMurdo Volcanic Group, Antarctica. *Bulletin of Volcanology*, *38*(1), 16–25.

Kyle, P. R., Moore, J. A., & Thirlwirl, M. F. (1992). Petrologic Evolution of Anorthoclase Phonolite Lavas at Mount Erebus, Ross Island, Antarctica. *Journal of Petrology*, *33*(4), 849–875. doi:10.1093/petrology/33.4.849

Le Bas, M. J., Le Maitre, R. W., Streckeisen, A., & Zanettin, B. (1986). A Chemical Classification of Volcanic Rocks Based on the Total Alkali-Silica Diagram. *Journal of Petrology*, *27*(3), 745–750. doi:10.1093/petrology/27.3.745

LeMasurier, W., & Thomson, J. W. (Eds.). (1990). *Volcanoes of the Antarctic Plate and Southern Ocean* (p. 487). Washington, DC: American Geophysical Union.

LINZ. (2014). Ross Island Topo Map 1:50,000. Land Information New Zealand.

MEVO. (2014). Mount Erebus Volcano Observatory. New Mexico Institute of Mining and Technology. Retrieved February 26, 2014, from http://erebus.nmt.edu/index.php

Moore, J. A., & Kyle, P. R. (1987). Volcanic Geology of Mount Erebus, Ross Island, Antarctica. In *Proceedings of the NIPR Symposium on Antarctic Geosciences* (pp. 48–65).

NIWA. (2014). CliFlo Database. Retrieved February 24, 2014, from http://cliflo.niwa.co.nz/

Panter, K. S., & Winter, B. (2008). Geology of the Side Crater of the Erebus volcano, Antarctica. *Journal of Volcanology and Geothermal Research*, *177*(3), 578–588. doi:10.1016/j.jvolgeores.2008.04.019

Peters, N., Oppenheimer, C., & Kyle, P. (2014). Autonomous thermal camera system for monitoring the active lava lake at Erebus volcano, Antarctica. *Geoscientific Instrumentation, Methods and Data Systems*, *3*(1), 13–20. doi:10.5194/gi-3-13-2014

Priestley, R. E. (1913). The ascent of Erebus, Deember 1912. In L. Huxley (Ed.), *Scott's Last Voyage* (pp. 274–280).

Rocchi, S., Armienti, P., D'Orazio, M., Tonarini, S., Wijbrans, J. R., & Di Vincenzo, G. (2002). Cenozoic magmatism in the western Ross Embayment: Role of mantle plume versus plate dynamics in

the development of the West Antarctic Rift System. *Journal of Geophysical Research*, *107*(B9), 2195. doi:10.1029/2001JB000515

Ross, J. C. (1847). *A Voyage of Discovery and Research in the Southern and Antarctic Regions* (Vol. 1., p. 366). London: John Murray.

Rowe, C. A., Aster, R. C., Kyle, P. R., Dibble, R. R., & Schlue, J. W. (2000). Seismic and acoustic observations at Mount Erebus Volcano, Ross Island, Antarctica, 1994–1998. *Journal of Volcanology and Geothermal Research*, *101*(1-2), 105–128. doi:10.1016/S0377-0273(00)00170-0

Stevens, N. F., Manville, V., & Heron, D. W. (2002). The sensitivity of a volcanic flow model to digital elevation model accuracy: experiments with digitised map contours and interferometric SAR at Ruapehu and Taranaki volcanoes, New Zealand. *Journal of Volcanology and Geothermal Research*, *119*, 89–105.

Wright, R., & Pilger, E. (2008). Satellite observations reveal little inter-annual variability in the radiant flux from the Mount Erebus lava lake. *Journal of Volcanology and Geothermal Research*, *177*(3), 687–694. doi:10.1016/j.jvolgeores.2008.03.005